Structural, Linear and Nonlinear Optical Properties of Some Al-free and Al-doped ZnO Nanopowder Samples

N.M. Moussa
Al-Azhar University Faculty of Science
F.M. Ebrahim
Al-Azhar University Faculty of Science
Hosam Mohamed Gomaa (h_goumaa@yahoo.com)
Independent Researcher, https://orcid.org/0000-0002-4806-7867
K. Adly
Suez Canal University Faculty of Science
M.Y Hassaan
Al-Azhar University Faculty of Science

Research Article

Keywords: ZnO, nanoparticles, optical properties, linear and nonlinear optics

Posted Date: July 6th, 2021

DOI: https://doi.org/10.21203/rs.3.rs-599622/v1

Structural, Linear and nonlinear optical properties of some Al-free and Al-doped ZnO nanopowder samples

N.M. Moussa[1], F.M. Ebrahim[1], Hosam Mohamed Gomaa[2], K. Adly[3], and M.Y Hassaan[1]

[1]Physics Department, faculty of science, Al azhar University, Cairo, Egypt

[2]Independent researcher, from Sakkara, Giza, Egypt

[3] Physics Department, faculty of science. Suez Canal University, Ismailia, Egypt

Abstract:

This research work aims to prepare and characterization some Al-doped ZnO nanoparticles. The co-precipitation method was used for preparing the desired samples, where ZnO replaced by $AlCl_3$. Then the resulted materials were characterized and their structural phases identified using the XRD technique, where eight crystalline phases were identified and then assigned to some of the interatomic planes, (100), (002), (101), (102), (110), (103), (112), and (201). Both the average crystalline size and the micro-strain were calculated for each sample, where it was found that both of them increase when Ai-content increases. UV-vis spectra showed an absorption peak centered at 3.34 eV which represents the optical bandgap of ZnO. Al-Impurities acted to improve and increase the value of the optical transmittance, especially in the visible light region. The increase of Al-content influenced, where their values increase when AL-content increases. the value of the calculated nonlinear refractive index may be considered promising for different optoelectronic applications.

Keywords: ZnO, nanoparticles, optical properties, linear and nonlinear optics

Corresponding author: Hosam M. Gomaa (Ph.D.),

Email: H_goumaa@yahoo.com WhatsApp. +201001381061

1. Introduction:

Nanomaterials and Nanocomposites are of high importance in different fields because of their potential applications, as storage energy devices, optoelectronic instruments, and solar cells. for example, Nanoparticles based on ZnO have used as a drug-delivery active medium in UV-region semiconductor lasers [1-6], where zinc oxide is a semiconductor oxide that has a wide direct bandgap of about 3.37 eV, and a large exciton binding energy of about 60 m eV [2, 3], at room temperature. Large numbers of publications stated that Nanoparticles based on Zinc metal oxide

with or without another metal oxide or more is considered as one of the most unique ways that provide what called long-lasting superior protection [7-9]. Also, it was found that when ZnO nanopowder mixes with other different ions acts to improve the optical, electrical, and catalytic properties of these ions [9], especially, when ZnO nanopowder doped with Al, where the resulted compound is conductive and transparent in the visible region, which suggests it be used in the transparent conductive pastes [10–11]. Therefore, in recent years the most researchers in the area of material science focused to develop new technics and experimental methods to obtain and fabricate ZnO nanostructures, like the co-precipitation, sol-gel, hydrothermal, and spray pyrolysis [12-18], Among all developed techniques the co-precipitation technique has attracted more attention because of its simplicity as well as its low cost, and effectiveness. Through inspecting the related previous articles, it was found that ZnO nanopowder doped with Al were reported only by a small number of researchers especially their optical properties in the UV-vis-near Ir region. So, this study is performed to prepare Al-free and Al-doped ZnO nanopowder using the co-precipitation method, to estimate the effect of Al-doping on structural and optical properties of ZnO nanopowder.

2. Experimental Work:

Pure and Al-doped ZnO nanoparticles were prepared by the chemical co-precipitation method. The materials used in this study without any purification include: Zinc acetate de hydrate {Zn $(CH_3COO)_2$ $.2H_2O$}, sodium hydroxide (NaOH), Aluminum chloride Anhydrous ($AlCl_3$). The experimental procedure for the preparation of pure ZnO and Al-doped ZnO samples are as follows: for the preparation of pure ZnO nanoparticles, 21.950 g of Zinc Acetate was dissolved in 100 ml distilled water and the solution mixed to be homogenous, then 16 g of sodium hydroxide was dissolved in distilled water. Next NaOH solution was added drop wise to obtain homogenous mixed solution, yielding a white precipitate. The white precipitate was stirred at room temperature for 2 hours. After that the solution was washed several times with distilled water and ethanol. The white powder was dried at 70 ºC for 3 hours followed by further heating at 400 ºC for 4 hrs, finely the white powder was grind using agate mortar. For the synthesis, Al doped ZnO nanoparticles, (2%) of Aluminum chloride was dissolved in (20 ml) distilled water, and (21.51 g) of zinc acetate dissolved in (80 ml) distilled water solution after stirring both solutions for half an hour the $AlCl_3$ was added dropwise to zinc acetate solution with continuous stirring then (16g) of sodium

hydroxide which dissolved in (100 ml) distilled water was added dropwise to this homogenous mixture to form a white precipitate. The solution with the white precipitate was processed as above to obtain Al-doped ZnO samples, table (1). The prepared samples were then characterized using different experimental methods, like the Powder X-ray diffractometer (XRD), at room temperature using a PW 1830 diffractometer with Cu Kα radiation (40 KV X 25 mA) and a graphite monochromatic, with 2θ values from 10 to 80 degrees. The optical measurements were obtained using Genway 6405-UV–visible Spectrophotometer which was used to get the optical UV–vis. Spectra, in the range 190 to 110 nm, at room temperature. While the FTIR spectra were recorded, at room temperature, using Fourier transform Infrared (FTIR) spectrometer in the range from 4000 to 400 cm^{-1}.

Table (1) Samples Composition

Sample Code	x wt (%)	ZnO wt %	$AlCl_3$ wt%
AZ1	0	100	0
AZ2	4	96	4
AZ3	6	94	6
AZ4	8	92	8

3. Results and discussion

3.1 Structural phase identification:

Figure (1) illustrates the normalized XRD patterns for the Aluminum-free sample and Aluminum-doped samples, where the pattern of each sample consists of eight- sharp peaks of different amplitudes and different positions. The existence of such a number of peaks means a variety of crystalline planes (hkl) that can be characterized according to their positions as in table (2). Based on the standard data on JCPDS card No. 36 –1451) all these data remark the structure matrix of Zinc oxide, ZnO, in other words, each sample has a pure hexagonal structure with well-developed crystallinity, where Al^{3+} ions were substituted into the sites of Zn^{2+} ions and/or incorporated into interstitial sites in the lattice without altering the hexagonal structure of ZnO [22]. it was observed when the content of Al^{3+} increased above 6% the positions of the crystalline phases/peaks exhibit a slight shift towards the higher diffraction's angle 2θ°, which may be attributed to the lattice shrinkage caused by the replacing of the Zn2+ (radius 0.74˚A) by Al3+ (radius 0.53˚A) [23-26].

Williamson-Hall (W-H) model, equation (1), was used to determine the average crystallite size (D) and the micro-strain (ε) for all samples;

$$\beta\cos\theta = K\lambda + 4\varepsilon \sin\theta \; D \quad (1)$$

$$\beta_{hkl} = \frac{K\lambda}{d_{hkl}\, Cos\, \theta_{hkl}} + 4\, \varepsilon \tan \theta_{hkl} \quad (2)$$

$$\beta_{hkl} Cos\, \theta_{hkl} = \frac{K\lambda}{d_{hkl}} + 4\, \varepsilon \,\mathrm{Sin}\, \theta_{hkl} \quad (3)$$

Where β is the full width at half maximum (FWHM) of the peak, θ is the Bragg's diffraction angle, K is the shape factor (K = 0.9), λ is the wavelength for CuKα radiation (λ = 1.54056 Å). Williamson [25-27] proposed the dependency of the diffraction line broadening on the crystallite size and strain contribution as shown in relation (2), which may further simplified to be as relation (3), Williamson Hall (W–H) equation. By plotting thee right hand side of relation (3), $\beta_{hkl} Cos\, \theta_{hkl}$, versus $4\,\mathrm{Sin}\, \theta_{hkl}$, as shown in figure (2), both micro-strain ε and the crystal size can be obtained. Where the slope of the resulted line gives the micro-strain ε, while the y-intercept gives the crystallite size. Figure (3) depicts that the obtained average crystallite size increase approximately linearly when ZnO is replaced by $AlCl_3$, where the Al-doped samples showed crystalline sizes larger than the Al-free one, which suggests the enhancement of crystalline quality. While figure (4) showed that the obtained micro-strain increases slightly when $AlCl_3$ content increases, which may be due to lattice mismatch with increasing the Al concentration.

Figure (5) exhibits Fourier-transform infrared spectroscopy, FTIR, for the Al-free sample and Al-doped samples in the wavelength range 400-4000 cm^{-1}. The absorption peak at 477 cm^{-1} is corresponding to the stretching mode of ZnO vibration. The absorption peak around 570 cm^{-1} attributed to presence of Al in ZnO lattice. The stretching mode of vibration bands due to C=O is observed between 1600-1400 cm^{-1}. A broad band of absorption were observed at 1097 cm^{-1} , 1384 cm^{-1} and 840 cm^{-1} effect the presence of H_2O (O-H) and CO_2 (C-O) that absorbed from the air, so can be ignored [28-29]. Those results confirmed the reducing the bonding force between acetate anion and zinc cations when the structural phase transformed from zinc acetate to ZnO, where the OH-groups gradually replaced with acetate groups, which removed completely to forming $Zn(OH)_2$, and hence/finally ZnO could be formed with the release more of acetate anion [30].

Table (2): detectable crystalline Planes

Phase No.	Position (2θ°)	Crystalline Plane (hkl)	Refs.
1	31.69	(100)	[19-20-21]
2	34.36	(002)	
3	36.18	(101)	
4	47.46	(102)	
5	56.52	(110)	
6	62.80	(103)	
7	67.88	(112)	
8	69.01	(201)	

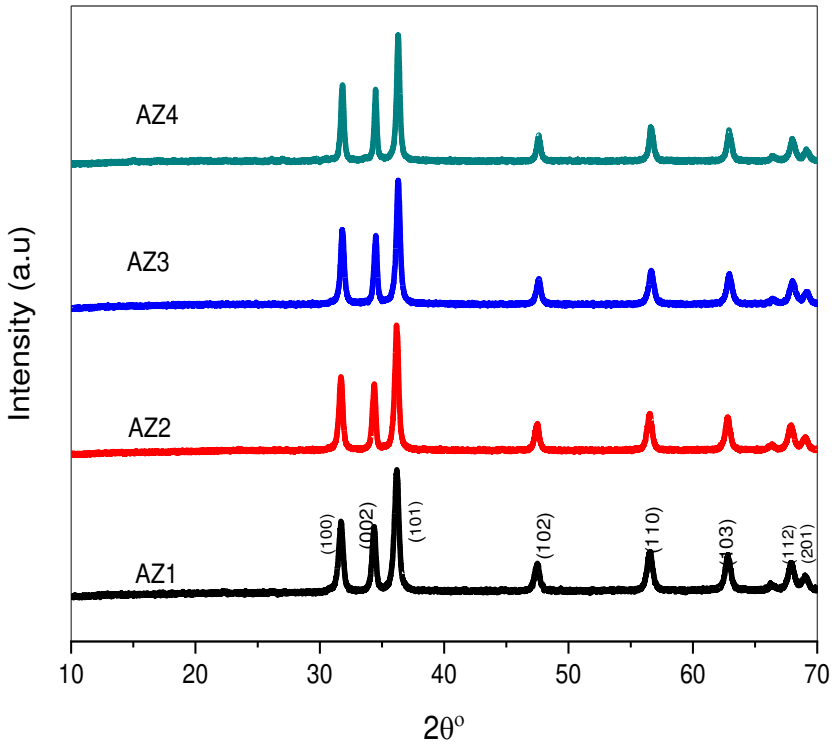

Figure (1): XRD patterns for all samples

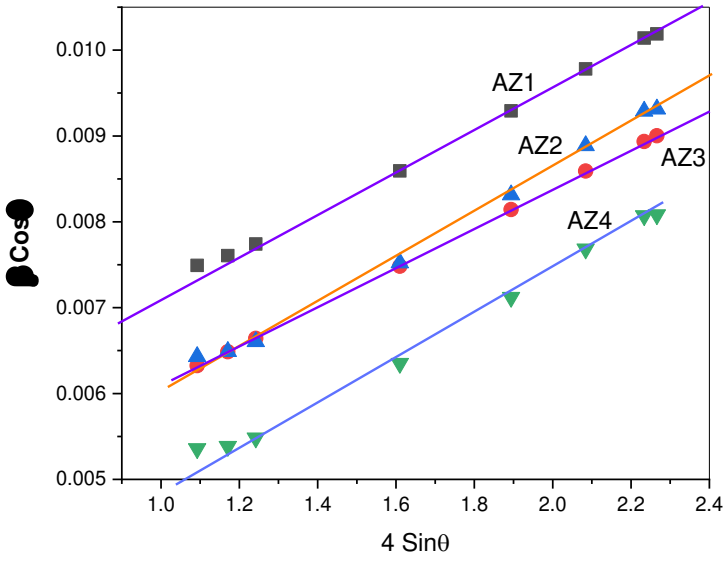

Figure (2): βCosθ versus 4Sinθ

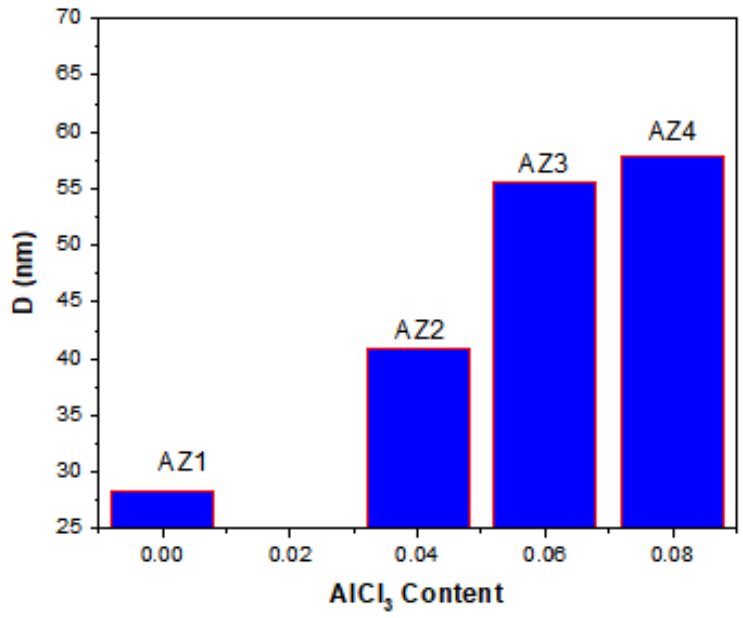

Figure (3): crystal size versesAlCl$_3$ concentration

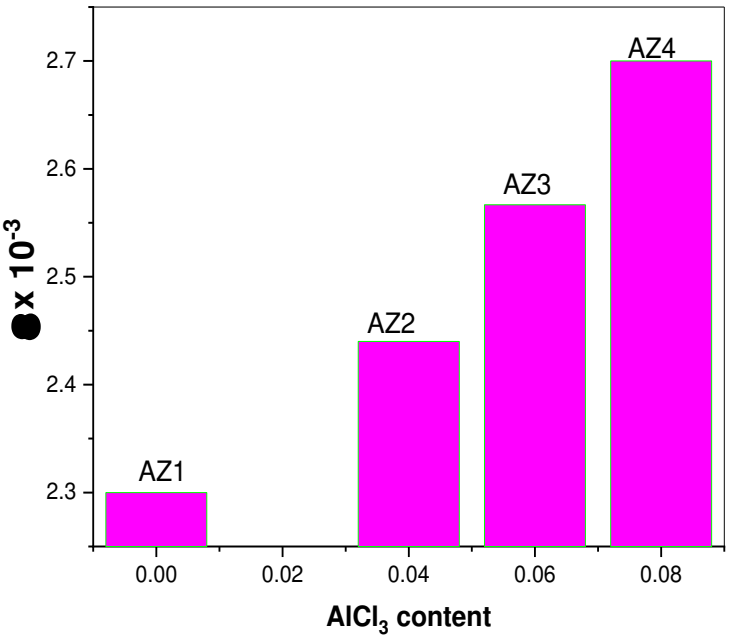

Figure (4): strain as a function of Al content.

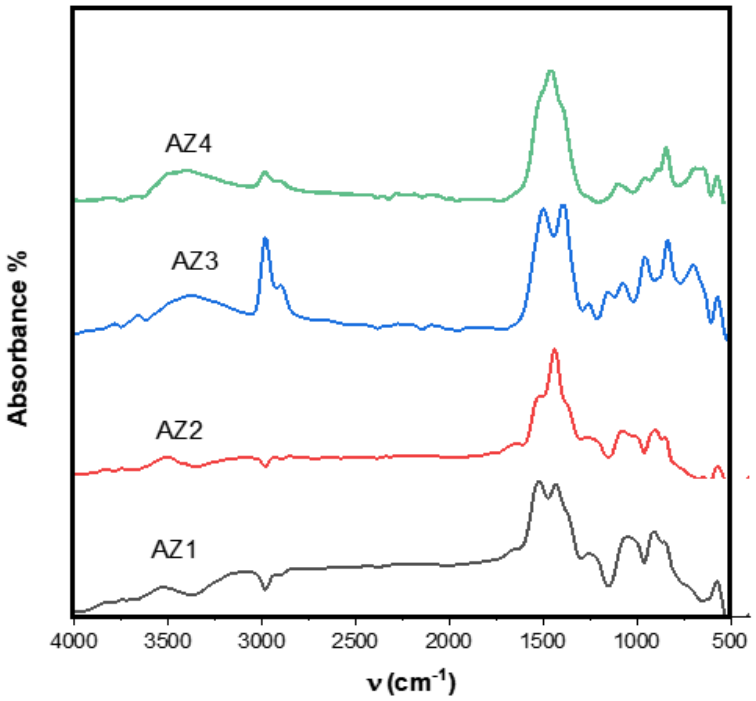

Figure (5) FTIR spectra for all the prepared samples.

3.2 UV-vis spectral analysis & Optoelectronic parameters:

The study of non-centrosymmetric substances like ZnO nanopowder is of most importance in estimate the electronic structure according to the optical properties, which are of high importance in updating both the electronics and optoelectronic devices for the different applications. In the current study some optical parameters like the transmittance, and absorbance were measured, while some others like absorption coefficient, linear refractive, and nonlinear refractive index were calculated [31-32-33]. For the studied samples both the optical absorbance and optical transmittance were measured then normalized, by dividing by the highest value, to avoid the instrumental errors. Figure (6) shows the variation of the normalized optical absorbance with the change in the wavelength of the incident light, where all samples exhibit approximately the same cut-off wavelength around 293 nm, in addition to an absorption peak at 373 nm which represent the optical bandgap of ZnO in the UV region. Figure (6) also clarify the effect of All-content on the optical absorption, where the increase of Al-content act to increase the optical absorption, such increase may be due to the observed increase in the average crystal size, as shown in figure (3). Figure (7) illustrates that all the studied samples have a wide transmission window extended over all the visible range, which may suggest them for multi applications in this region. According to relation (4), [34], both the optical absorption of each sample and its thickness (t) were used to calculate its absorption coefficient α, which is an important factor for determining the energy bandgaps for both direct and indirect allowed transitions, by using Tauc's relation (5), [35-36];

$$\alpha = 2.303 * \frac{A}{t} \quad (4)$$

$$\alpha E = \alpha_o \, (E - E_g)^{j} \quad (5)$$

Where α_o is a constant called band tailing parameter, E_g is the optical energy gap, and j is the power factor of the transition mode. The values of j for both direct and indirect transitions are ½ and 2, respectively. To determine the value of the energy bandgap for indirect allowed transition the quantity $(\alpha E)^{0.5}$ was plotted versus the photon energy E, as shown in figure (8), where the direct bandgap energy is equal to the intercept of the straight portion curve with the x-axis. And by the same method, it can determine the value of the bandgap energy for the direct allowed transition by plot $(\alpha E)^2$ versus E, as shown in figure (9). The calculations showed that the replacement of ZnO

by $AlCl_3$ act to increase the optical bandgaps from 3.53 to 3.75 for the indirect allowed electronic transitions, and from 3.75 to 4.1 eV for the direct allowed electronic transitions.

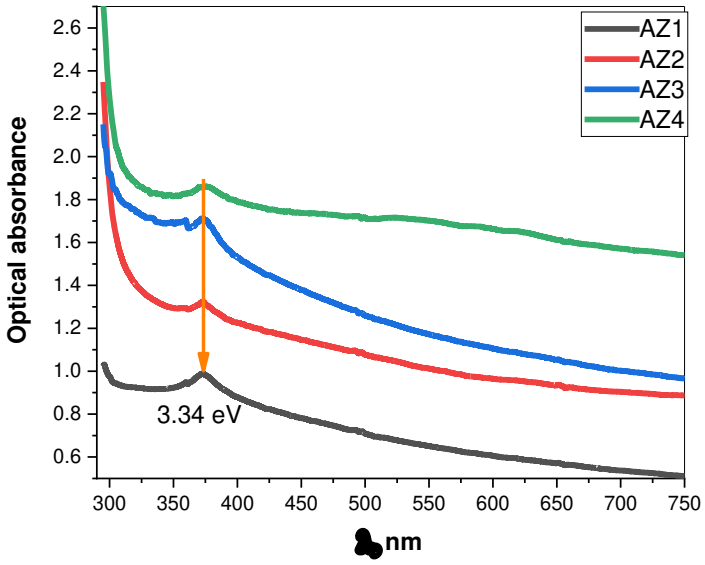

Figure (6): The normalized Absorbance, for all the prepared samples.

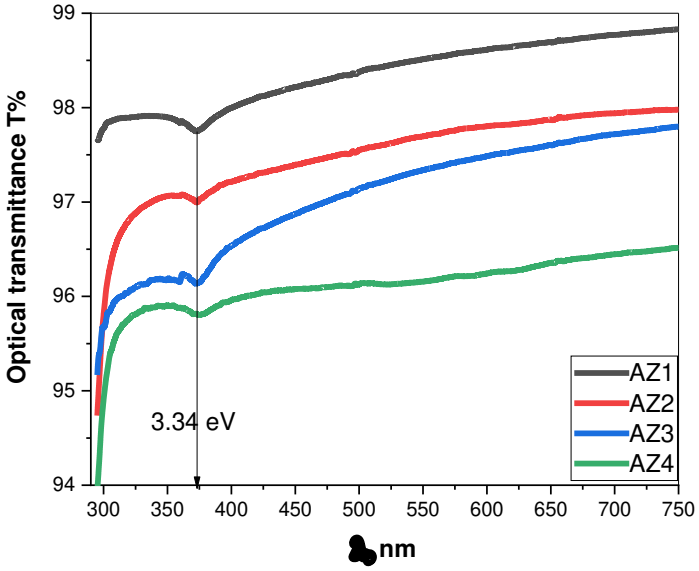

Figure (7): The optical transmittance, for all the prepared samples

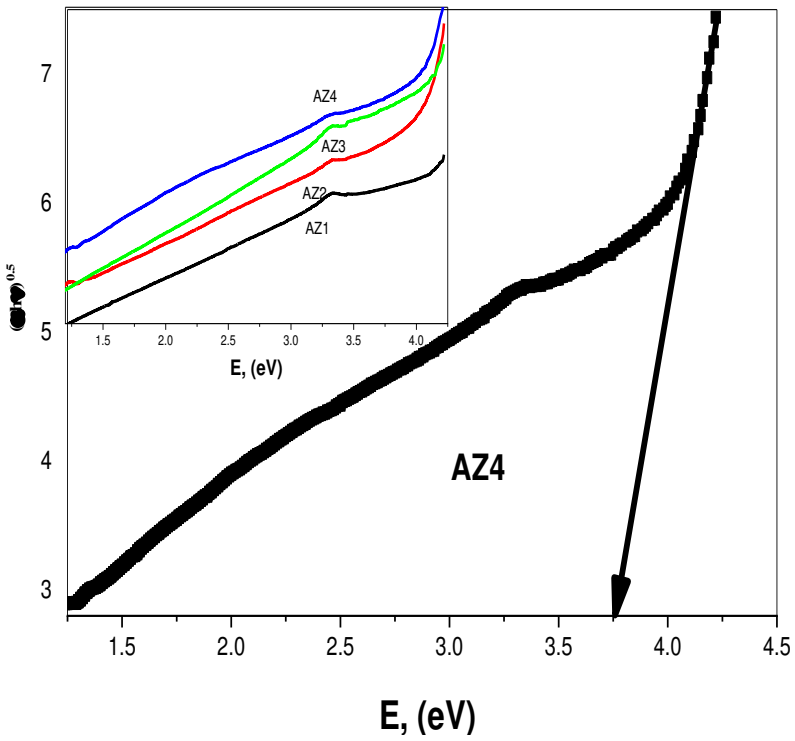

Figure (8): $(\alpha E)^{0.5}$ versus E=hν for all the prepared samples

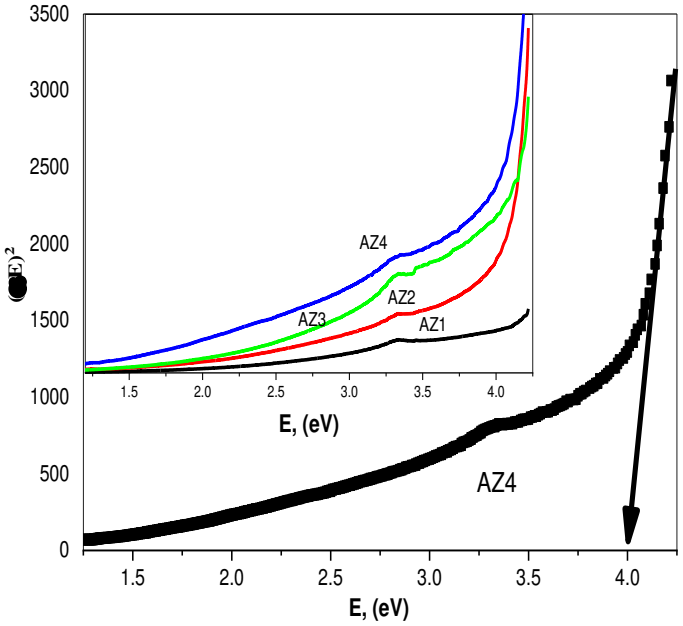

Figure (9): $(\alpha E)^{2}$ versus (E=hν), for all the prepared samples

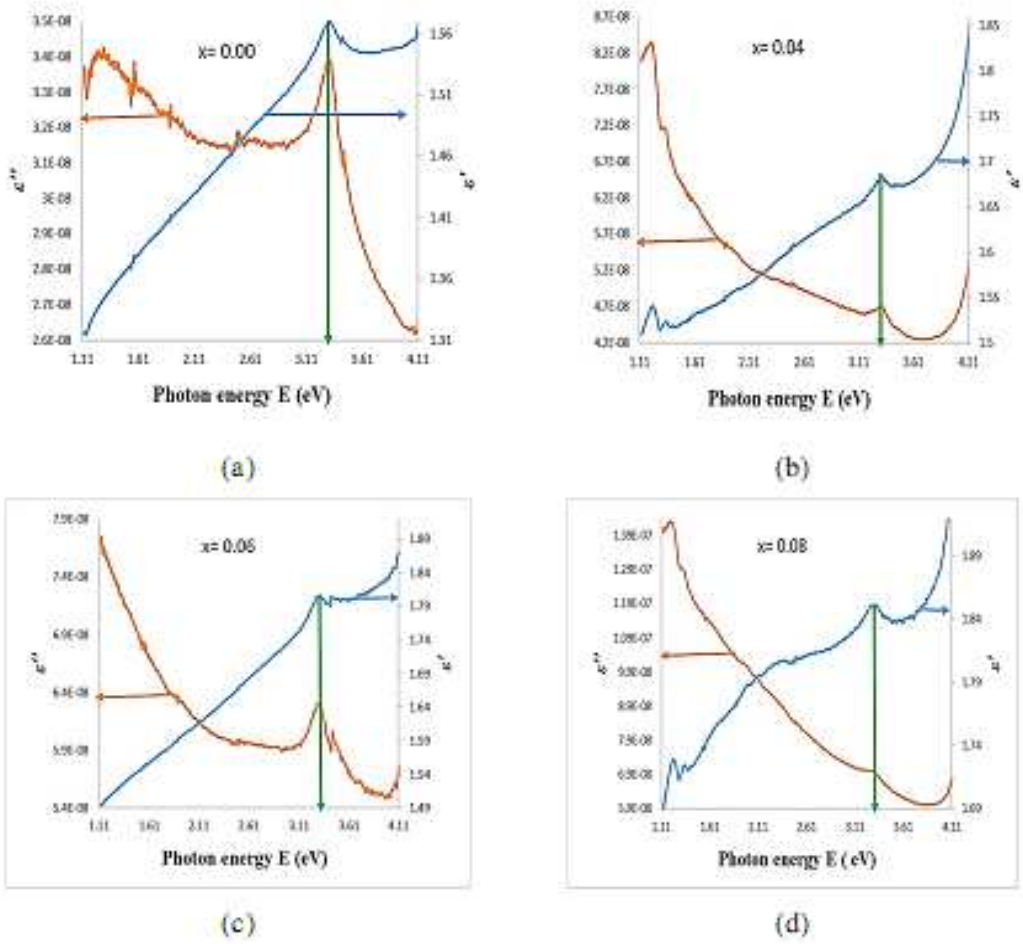

Figure (10): ($\boldsymbol{\varepsilon'}$) and ($\boldsymbol{\varepsilon''}$) as a functions of the photon energy

Based on the measured optical parameters the optical dielectric relaxation can be organized in view of the real ($\boldsymbol{\varepsilon'}$) and imaginary ($\boldsymbol{\varepsilon''}$) components of the optical dielectric constant ε* [37-38]. Where for unfree damper, the real component ($\boldsymbol{\varepsilon'}$) characterize the damping of the light propagation thorough the material/medium. Also this component, which related to the energy stored within the medium, can be considered as accounts for electromagnetic dispersions. In other side, the imaginary component is considered as a damping factor describes the amount of energy loss and/or absorbed within the medium [37-38].

$$K(E) = \frac{\alpha\, hc}{4\pi E} \tag{6}$$

$$R = \frac{100 - A - T\%}{100} \tag{7}$$

$$n = \frac{1+R}{1-R} + \sqrt{\frac{4R}{(1-R)^2} + K^2} \quad (8)$$

$$\varepsilon' = n^2 - K^2 \quad (9)$$

$$\varepsilon'' = 2nK \quad (10)$$

$$\varepsilon^* = \varepsilon' + j\,\varepsilon'' \quad (11)$$

Figures 10(a-d) represents the vibration of $\boldsymbol{\varepsilon'}$ and $\boldsymbol{\varepsilon''}$ with the energy of the incident photons for x = 0, 0.04, 0.06 and 0.08, respectively. Where the real component $\boldsymbol{\varepsilon'}$ increases while the imaginary component (ε") decreased, in such a way where both of them show a peak in the same position (3.3 eV). Such a result can be used to obtain the average plasma frequency $f_o = 8\ x\ 10^{14}\ Hz$ which is higher value expresses the existence of a high concentration of free carriers [37].

3.4 Nonlinear optical parameters

$$\chi^{(1)} = \frac{n^2-1}{4\pi} \quad (12)$$

$$\chi^{(3)} = 1.7\ x\ 10^{-10}\ (\chi^{(1)})^4 \quad (13)$$

$$n_2 = \frac{12\pi\,\chi^{(3)}}{n} \quad (14)$$

Frequency conversion materials especially nanopowder semiconductors are important for nonlinear optical applications, so it is useful to identify the nonlinear properties of the studied samples to recognize if they are suitable for nonlinear devices and applications or not. For this promotion, it's favorable to use the Z-scan technique but it's not available for now at least so the set of the previous relations should be used to obtain the nonlinear parameters of the studied samples based on UV-vis measurements. Figure (11) shows the calculated nonlinear refractive index n2, where the obtained values for the Al-free sample and Al-doped samples is better than those reported previously [38-39], which may suggest these samples for nonlinear applications.

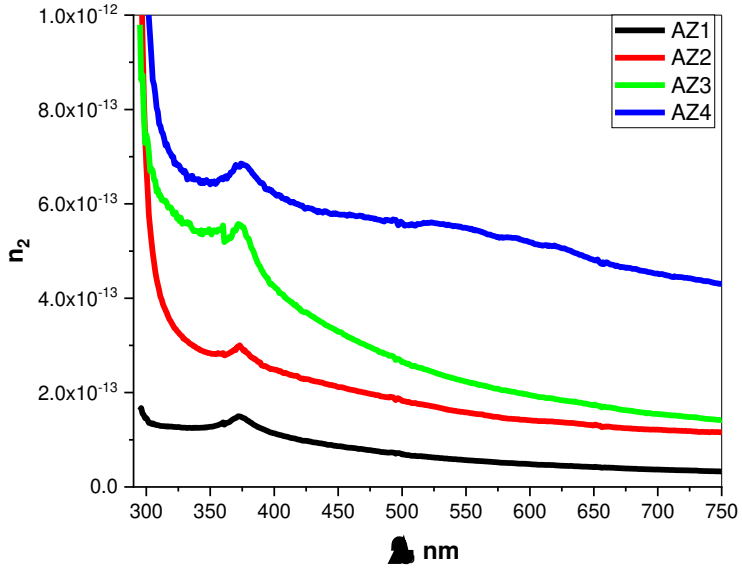

Figure (11): Nonlinear refractive index n2

Conclusion:

Four Nano composite powder samples have been prepared base on the chemical reaction formula, $Zn_{1-x}Al_x$, where $0 \leq x \leq 0.1$ in wt% using the co-precipitation method. The substitution of ZnO by Al setup seven crystalline phases/planes (100), (002), (101), (102), (110), (103), and (201). For characterizing the obtained samples the average crystalline size and the micro-strain were calculated and were found to be increase with increasing Al content. All the studied samples exhibited high optical transparency in the visible light region. Direct and indirect energy gaps, the absorption coefficient, and nonlinear refractive index were calculated and showed increasing values with increasing Al content. The obtained results are considered promising for different optoelectronic applications.

Conflict of interest:

All the authors declare that there is no conflict of interest.

4. References

1. Coleman, VA., Bradby, JE., Jagadish, C., Munroe, P., Heo, YW., Pearton, SJ., Norton, DP., Inoue, M., Yano, M., 2005
2. Yadav, BC. Richa Srivastava, and Alok Kumar, 2007. International Journal of Nanotechnology and Applications. ISSN 0973-631, 1-11.
3. Bouvy, C., Marine, W., Sporken, R., Su, BL., 2007. Colloids and Surfaces A: Physicochem. Eng Aspects 300, 145 149.
4. Pivin, J.C., Socol, G., Mihailescu, I., Berthet, P., Singh, F., Patel, M.K.: Thin Solid Films 517, 916–922 (2008).
5. Sato, K., Yoshida, H.K.: Jpn. J. Appl. Phys. 39, L555–L558 (2000).
6. Avinash K, Saritha D, Joginder S, Mayank K, Vishnu dev G. Synthesis and characterization of ZnO nanoparticles. Ori-ental Journal of Chemistry. 2014; 30.
7. Alessio B. Maximilian Du Pierandrea Lo Nostro Æ Pie-ro Baglioni. Synthesis and characterization of zinc oxide nanoparticles: Application to textiles as UV-absorbers. J Nanopart Res; 2008; 10:679-89. DOI 10.1007/s11051-007- 9318-3
8. H. Serier, M. Gaudon, M. Ménétrier, Al-doped ZnO powdered materials: Al solubility limit and IR absorption properties, Solid State Sci.11 (7) (2009) 1192–1197.
9. B. Zhang, N. Binh, K. Wakatsuki, Y. Segawa, Y. Yamada, N. Usami, M. Kawasaki, H .Koinuma, Formation of highly aligned ZnO tubes on sapphire (0 0 0 1) substrates, Appl. Phys. Lett. 84 (20) (2004) 4098–4100.
10. E. Hammarberg, A .Prodi-Schwab, C. Feldmann, Microwave-assisted polyol synthesis of aluminium-and indium-doped ZnO nanocrystals, J. Colloid Interface Sci.334 (1) (2009)29–36.
11. L. Ji, W. Shih, T. Fang, C. Wu, S. Peng, T. Meen, Preparation and characteristics of hybrid ZnO-polymer solar cells, J. Mater. Sci. 45(12) (2010) 3266–3269.
12. Boshra Ghanbari Shohany and Ali Khorsand Zak, Ceramics International, https://doi.org/10.1016/j.ceramint.2019.11.051
13. **T**. Ogi, D. Hidayat, F. Iskandar, A. Purwanto, K. Okuyama, Direct synthesis of highly crystalline transparent conducting oxide nanoparticles by low pressure spray pyrolysis, Adv. Powder Technol. 20(2)(2009) 203–209.

14. H. Zhang, D. Yang, S.Li, X. Ma, Y. Ji, J. Xu, D. Que, Controllable growth of ZnO nanostructures by citric acid assisted hydrothermal process, Mater. Lett .59 (13) (2005) 1696–1700.
15. Zhou H M, Yi D Q, Yu Z M, Xiao L R and Li J 2007 Thin Solid Films 515 6909.
16. Chen K J, Fang T H, Hung F Y, Ji LW, Chang S J, Young S J and Hsiao Y J 2008 Appl. Surf. Sci. 254 5791
17. Li QH, Zhu D, Liu W, Liu Y, Ma XC (2008) Optical properties of Al-doped ZnO thin films by ellipsometry. Appl Surf Sci 254 (10):2922–2926
18. Ehrmann N, Reineke-Koch R (2010) Ellipsometric studies on ZnO:Al thin films: refinement of dispersion theories. Thin Solid Films 519(4):1475–1485
19. L.H. Van, M.H. Hong, J. Ding, Structural and magnetic property of Co-doped- ZnO thin films prepared by pulsed laser deposition, J. Alloys Comp. 449 (1) (2008) 207–209.
20. K. Gherab, Y. Al-Douri, C.H. Voon, U. Hashim, M. Ameri, A. Bouhemadou. Result in Physics 7 (2017) 1190-1197
21. P. Swapna and S. Venkatramana Reddy*. Synthesis and Characterization of Al Doped and (Co, Al) co-doped ZnO Nanoparticles via Chemical co-precipitation Method. Asian Journal of Nanoscience and Materials, 2018, **2**(1), 111-119.
22. Mallika AN, Ramachandra Reddy A, Sowribabu K, Venugopal Reddy K. Structural and optical characterization of Zn0.95_xMg0.05AlxO nanoparticles. Ceram Int 2015; 41:9276–84
23. Kadam P, Agashe C, Mahamuni S (2008) J Appl Phys 104: 103501. doi: 10.1063/1.3020527
24. Park KC, Ma DY, Kim KH (1997) Thin Solid Films 305:201.
25. Navale SC, Ravi V, Mulla IS, Gosavi SW, Kulkarni SK (2007) Sens Actuators B 126:382. doi: 10.1016/ j.snb. 2007.03.019
26. Reddy AJ, Kokila MK, Nagabhushana H, Chakradhar RPS, Shivakumara C, Rao JL, et al. Structural, optical and EPR studies on ZnO: Cu nanopowders prepared via low temperature solution combustion synthesis. J Alloys Compd 2011; 509:5349–55.
27. R. Bhargava, P.K. Sharma, S. Kumar, A.C. Pandey, N. Kumar, Consequence of doping mediated strain and the activation energy on the structural and optical properties of ZnO:Cr nanoparticles, Journal of Solid State Chemistry 183 (2010) 1400.

28. Gnachari S.V. Bhat r., Deshpande R., Venkataraman A., Recent Res. Sci. Tech., 4 (2012), 50.
29. Zahraa M. AL-Asady, Ali H. AL-Hamdani, and Mohammed A. Hussein, AIP Conference Proceedings 2213, 020061 (2020); https://doi.org/10.1063/5.0000259 .
30. Zohra N. Kayani, Fareeha Naz, Saira Riaz, Shahzad Naseem, Journal of Saudi Chemical Society (2017) 21, 425-433.
31. Hossam Mohamed Gomaa, I. S. Ali, Ammar S. Morsy and M. I. Sayyed, J. of Applied Physics A, (2020), 126:384, https://doi.org/10.1007/s00339-020-03552-z
32. M. Y. Hassaan, H. A. Saudi, Hossam M. Gomaa and Ammar S. Morsy, J. of Materials and Applications 2020;9(1):46-54, https://doi.org/10.32732/jma.2020.9.1.46
33. Hossam M. Gomaa, M. Y. Hassaanm H. A. Soudi and Ammar S. Morsy, J. of Applied Physics A, (2020), 126:391, https://doi.org/10.1007/s00339-020-03582-7
34. S.M. Elkatlawy, et al., Structural properties, linear, and non-linear optical parameters of ternary Se80Te(20−x) Inxchalcogenide glass systems, Bol. Soc. Esp. Cerám. Vidr. (2020), https://doi.org/10.1016/j.bsecv.2020.09.007
35. M. Y. Hassaan et al., J. of Materials and Applications (2020) ;9(1):46-54
36. El-Mansy MK, Gomaa H. M, Hendawy N, Morsy AS. Effect of exchange of Bi^{+3} by Nb^{+5} on the structural and optical properties of some $(BBiNb)_2 O_7$ CaO oxide glasses. J. of Non-Crystalline Solids. 2018;485:42-46
37. Ahmed Saeed Hassanien and Ishu Sharma, J. of Optik, 200 (2020), 163415
38. V. Ganesh, I. Yahia, S. Alfaify, M. Shkir, Sn-doped Zno nanocrystalline thin flms with enhanced linear and nonlinear optical properties for optoelectronic applications. J. Phys. Chem. Solids 100, 115–125 (2017). https://doi.org/10.1016/J.Jpcs.2016.09.022
39. Ahmed Saeed Hassanien, J. of Alloys Compd. 671, (2016) 566-578.